Journal of Materials Chemistry C

Quenching of Photoluminescence in a Zn-MOF Sensor by Nitroaromatic Molecules

Journal:	*Journal of Materials Chemistry C*
Manuscript ID	TC-ART-12-2018-006281.R1
Article Type:	Paper
Date Submitted by the Author:	20-Jan-2019
Complete List of Authors:	Jensen, Stephanie; Wake Forest University, Tan, Kui; University of Texas-Dallas, Material Science and Engineering Lustig, William; Rutgers University Kilin, Dmitri; North Dakota State University, Department of Chemistry and Biochemistry Li, Jing; Rutgers University, Chemistry and Chemical Biology Chabal, Yves; University of Texas at Dallas, Thonhauser, Timo; Wake Forest University

Quenching of Photoluminescence in a Zn-MOF Sensor by Nitroaromatic Molecules

S. Jensen,[1,2] K. Tan,[3,*] W. Lustig,[4,*] D. Kilin,[5] J. Li,[4] Y. J. Chabal,[3] and T. Thonhauser[1,2,†]

[1]*Department of Physics, Wake Forest University, Winston-Salem, NC 27109, USA*
[2]*Center for Functional Materials, Wake Forest University, Winston-Salem, NC 27109, USA*
[3]*Department of Materials Science and Engineering, University of Texas at Dallas, Richardson, TX 75080, USA*
[4]*Department of Chemistry and Chemical Biology, Rutgers University, Piscataway, NJ 08854, USA*
[5]*Department of Chemistry and Biochemistry, North Dakota State University, Fargo, ND 58108, USA*

(Dated: January 20, 2019)

We uncover the exact mechanisms that lead to a quenching of the photoluminescence in a Zn-based metal organic framework (MOF) material upon nitroaromatic molecule adsorption. We present evidence based on *ab initio* simulations, coupled with *in situ* IR spectroscopy and photoluminescence measurements, showing that quenching occurs as the result of a shift of the lowest unoccupied orbital from the MOF host to the guest molecule. Our results provide a mechanistic understanding of quenching of photoluminescence in MOFs and are of importance for chemical sensing applications, where they aid the design of novel MOFs with increased sensing selectivity.

I. INTRODUCTION

Metal organic framework (MOF) materials are synthesized via self assembly from metal ions (forming the primary building blocks) and organic linkers (serving as the secondary building blocks). Due to the wide variety of available building blocks, MOFs encompass a vast amount of already synthesized materials with a large variety of different properties and applications, including gas storage and sequestration,[1–9] catalysis,[10–13] drug delivery,[14] luminescence,[15,16] and multiferroics.[17–19] Of particular interest are MOFs with photoluminescent properties, with applications in optoelectronics, bioimaging, and chemical sensing.[20–26] For the latter, the underlying idea is that the guest molecules to be sensed induces observable changes in the photoluminescent response of a MOF, such as *quenching* (which decreases or completely eliminates the light emitting property of the MOF upon guest molecule adsorption) and *enhancement* (which either induces a non-emitting MOF to fluoresce or noticeably increases the intensity of light emission of an already fluorescing MOF upon molecule adsorption). Although significant progress has been made in understanding and tuning photoluminescent MOFs recently,[27] unfortunately the fundamental electronic-structure mechanisms and atomic scale processes that change the photoluminescence upon guest molecule adsorption are still not fully understood. Experimental studies suggest various possible mechanisms,[26,28–32] but a deterministic approach to proof or disproof them is still missing.

MOFs have shown a variety of different mechanisms for emitting light such as metal-to-ligand charge transfer (MLCT), ligand-to-metal charge transfer (LMCT), and ligand-to-ligand charge transfer (LLCT).[27] In this paper, we focus on LLCT photoluminescent MOFs, most of which are composed of a d^{10} metal and two fluorophore (light emitting) organic ligands. The fully occupied d orbitals allow the metal or metal node to electronically insulate the two organic ligands. When the MOF absorbs light, an electron is excited from one organic linker (the donor) to the other organic linker (the acceptor). Because the metal already contains fully occupied valence orbitals, the electron and hole are essentially trapped on the respective organic linkers. Eventually, after relaxation, the electron and hole recombine emitting light, often at a wavelength equal to the energy difference of the highest occupied molecular orbital (HOMO) and lowest unoccupied molecular orbital (LUMO) of the framework. To utilize this mechanism for sensing applications, the MOF should ideally (i) absorb light at a particular, easy to use wavelength, (ii) emit in the visible range,

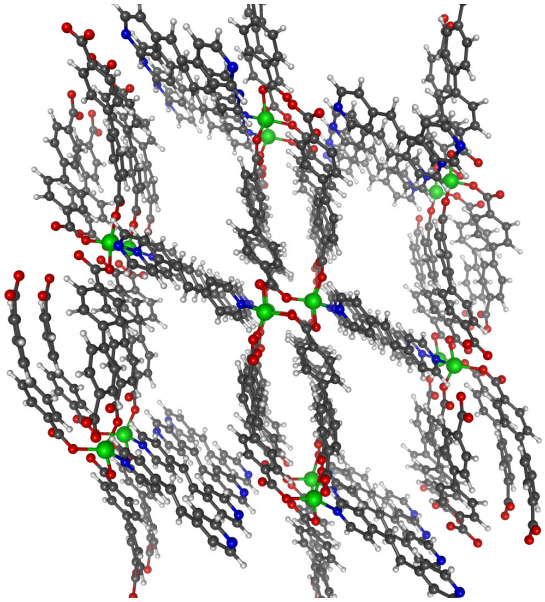

Figure 1. The MOF structure considered in this study, RPM3-Zn, is a selective quencher of photoluminescence upon adsorption of nitroaromatic compounds. Atoms are colored as follows: C (grey), N (blue), O (red), Zn (green), and H (white).

and (iii) have a clear, highly selective response for different molecules of interest. While these aspects have been tuned for many MOFs,[27] their effective tailoring for sensing applications is only possible through a fundamental understanding of the mechanisms involved.

A number of theoretical hypotheses enable the interpretation of experimentally observed photoluminescence and give rise to the computational modeling of photoluminescence in MOFs. First, Kasha's rule[33] states that photoluminescence will only occur in appreciable yield from the lowest excitation (LUMO to HOMO). Second, photoluminescent linewidth broadening occurs as thermal fluctuations and nuclear reorganization of ions, altering the energy of electronic states and necessitating calculations beyond static ground-state optimization. Here, we combine *ab initio* methods with synthesis, vibrational spectroscopy, and photoluminescence experiments to address this question in regards to photoluminescence quenching in MOFs upon guest adsorption and provide a fundamental mechanistic description on the atomic scale. In particular, we uncover and analyze in detail the mechanism of the photoluminescence response of the prototypical quenching MOF RPM3-Zn (Fig. 1), i.e. $Zn_2(bpdc)_2(bpee)$ [bpdc = 4,4′-biphenyldicarboxylate; bpee = 1,2-bipyridylethene], known to be a selective quencher upon adsorption of explosive compounds, in particular 2,4-dinitrotoluene (DNT), which is a precursor compound to TNT.[34]

II. METHODS

A. Computational Details

Calculations were performed at the density functional theory (DFT) level in VASP,[35,36] using the vdW-DF[37–40] exchange-correlation functional to incorporate the long-range van der Waals interactions between the MOF and guest molecules. Standard VASP PAW pseudopotentials were implemented with a 600 eV energy cutoff. Only the Γ-point was used due to the size of the RPM3-Zn unit cell with 156 atoms, comprising a bulk MOF model with periodic boundary conditions. Electronic relaxations were carried out until the SCF loops reached an energy convergence of less than 1×10^{-4} eV and structural relaxations were performed until forces on all atoms were below 1 meV/Å. Vibrational frequencies were calculated in order to verify experimental peak assignments and confirm guest/MOF interactions. The finite differences method was utilized in VASP with atoms individually displaced by 0.01 Å and the resulting dynamical matrix was diagonalized under the constraints of applicable sum rules.

Two main approximations are made when calculating the optical properties: the independent orbital approximation (i.e. the transition probability is calculated between two specified states) and the dipole approximation (i.e. the electromagnetic wavelength is much larger than the length of the molecular system). While static calculations are sufficient for finding the ground-state geometry, studying the interaction of DNT with RPM3-Zn, and calculating the phonon modes, line broadening of photoluminescence necessitates sampling the optical properties along the nuclear trajectory $\mathbf{R}_\mathrm{I}(t)$. The main ingredient for calculating optical spectra is the oscillator strength, given by

$$f_{ij}\big(\{\mathbf{R}_\mathrm{I}(t)\}\big) = \frac{4\pi m_e \omega_{ij}}{3\hbar e^2}\left|\mathbf{D}_{ij}\big(\{\mathbf{R}_\mathrm{I}(t)\}\big)\right|^2 , \qquad (1)$$

where e and m_e are the charge and mass of the electron, $\hbar\omega_{ij} = \varepsilon_i - \varepsilon_j$ is the energy difference between electronic states i and j, $\{\mathbf{R}_\mathrm{I}(t)\}$ is the set of all ionic positions at time t, and $\mathbf{D}_{ij}$ is the transition dipole moment

$$\mathbf{D}_{ij}\big(\{\mathbf{R}_\mathrm{I}(t)\}\big) = e\int \psi_i^*\big(\{\mathbf{R}_\mathrm{I}(t)\}\big)\ \mathbf{r}\ \psi_j\big(\{\mathbf{R}_\mathrm{I}(t)\}\big)\ d^3r\ . \qquad (2)$$

To capture the dynamics of the system as well as finite temperature effects, we follow the methodology in Ref. [41] and gather the necessary statistics by evaluating the oscillator strengths for all time steps along an *ab initio* molecular dynamics (MD) trajectory. In particular, we use VASP to perform Born-Oppenheimer MD for 1000 time steps (fs) at $T = 300$ K ($T = 50$ K and 550 K were also computed to study the effect of vibrations on computed oscillator strengths) using the standard *ab initio* Verlet algorithm with total free-energy conservation, resulting in a 1 ps trajectory. At each of the 1000 time steps we calculate f_{ij} for all possible transitions, i.e. i runs over all occupied states (268 states) and j runs over all unoccupied states (92 states). Albeit, the most interesting transitions in the visible range occur within 10 states of the valence and conduction band edges. Photolumincescence in MOFs is typically dominated by transitions between the LUMO and HOMO[33] and we will provide evidence below that this is also the case for RPM3-Zn. Photoluminescence spectra are then calculated from the oscillator strengths of the LUMO to HOMO transition, overlaying a Gaussian, and summing over all time steps of the trajectory.

As evident from Eqs. (1) and (2), f_{ij} depends on the orbitals of both states i and j and the difference in their energies. DFT is not the correct level of theory to capture such energy differences across the band gap accurately, but the shape of the Kohn-Sham orbitals ψ_i^KS is well approximated and the resulting $\mathbf{D}_{ij}$ are meaningful. GW calculations were attempted for the full RPM3-Zn system, but the unit cell is too large for this level of calculation. As a result, we calculate the $\mathbf{D}_{ij}$ at the KS level and for the f_{ij} we used the "scissors" operator as a post-processing step, adjusting the KS band gap to our experimentally measured one. This approach was verified by comparing with significantly more expensive hybrid-functional calculations on a number of snapshots along our MD trajectory using HSE06,[42] which can provide an improved description of excited states.[43] Our scissors approach results in oscillators strengths that are within 1%

of the hybrid functional results in general and, interestingly, even less for LUMO to HOMO transitions.

From the data gathered throughout the MD simulations we can also calculate the non-adiabatic electronic couplings and, in turn, the non-radiative lifetime of the various excited electron and hole states. Non-adiabatic electronic couplings are calculated by going beyond the Born-Oppenheimer approximation of treating the nuclear motion and electronic structure separately by assessing the response of the electronic degrees of freedom to the nuclear motion. The nuclear trajectory is interfaced with a thermostat, keeping kinetic energy constant (thermal bath). On-the-fly non-adiabatic couplings are computed along the nuclear trajectory,

$$\mathbf{V}_{ij}^{\mathrm{NA}}(t) = -\frac{i\hbar}{2\Delta t}\int \psi_i^*\big(\{\mathbf{R}_{\mathrm{I}}(t)\}\big)\,\psi_j\big(\{\mathbf{R}_{\mathrm{I}}(t+\Delta t)\}\big)\,d^3r\,, \quad (3)$$

serving as a measure of electron-phonon coupling, which is the basis for calculating the relaxation rates and dynamics. The underlying theory, methodology, and code for the electronic coupling calculations are described in detail elsewhere;[41,44] some further details of its applicability can be found in the SI. Our simulations confirm that non-radiative relaxation of electrons and holes from the excited state to LUMO and HOMO, respectively, happens on a femtosecond to picosecond time-scale. Thus, this provides *a posteriori* justification for our focus on only the LUMO to HOMO transition when studying photoluminescence, which happens on a nanosecond time-scale.

The ionic vibrational variance during the molecular dynamics trajectory is calculated in the form of the mean square displacement matrix **U**, as described by Svane and Walsh.[45] The matrix elements $U_{\alpha\beta}$ are defined as

$$U_{\alpha\beta} = \big\langle (u_\alpha - \bar{u}_\alpha)(u_\beta - \bar{u}_\beta)\big\rangle\,, \quad (4)$$

where α and β are coordinate axes and $\bar{u}_\alpha$ refers to the average position along the α axis. These values are calculated for all atoms of the system along the x, y, and z axes using the position of the atoms at each time step of the 1000 fs molecular dynamics trajectory. The matrix elements are then used to create thermal ellipsoid images.

B. Characterization

Photoluminescence Spectra: All experimental photoluminescence spectra were collected at room temperature using a Varian Cary Eclipse fluorescence spectrometer under 320 nm excitation. A freshly activated sample of RPM3-Zn was used to collect the experimental RPM3-Zn emission spectrum, while the experimental DNT+RPM3-Zn emission spectrum was collected using the same freshly activated RPM3-Zn sample following incubation in a saturated DNT atmosphere until the emission quenching was maximized (approximately 10 minutes).

Absorption Spectra: The diffuse reflectance spectra were collected on a Shimadzu UV-3600 spectrophotometer at room temperature. The DNT+RPM3-Zn sample was created by enclosing the RPM3-Zn sample within a small jar under an atmosphere saturated with DNT vapor for 48 hours. Because the samples are solid, the diffuse reflectance spectra were collected and the Kubelka Munk (KM) equation was used to convert the reflectance data into a function that is directly proportional to the absorbance coefficient.

IR Spectra: An as-synthesized RPM3-Zn sample was immersed into 20 mL of methanol for 3 days, followed by a 4-day immersion in 20 mL of dichloromethane. After filtering, 2 mg of dried sample was lightly pressed onto a KBr pellet (1.3 cm diameter, 1–2 mm thick) and loaded into a vacuum cell (Specac product. P/N 5850c, UK). The cell was installed at the focal point of the sample compartment of the infrared spectrometer (Nicolet 6700, Thermo Scientific, US) equipped with a liquid N_2-cooled MCT-A detector. The sample was annealed to 150°C for $>$ 3 hours for activation and cooled back to room temperature to record the IR spectrum before exposure to DNT vapor. To increase the amount of adsorption, the DNT powder was vaporized in a metal container at over 160°C. The sample was placed above the metal container for 5 minutes to adsorb the DNT vapor. The DNT exposed sample was loaded into the vacuum cell and a 20-loop IR spectrum (100 scans per loop) was recorded under evacuation for 20 minutes.

C. Synthesis

RPM3-Zn was synthesized solvothermally.[34] $Zn(NO_3)_2{\cdot}6H_2O$ (0.30 mmol), H_2bpdc (0.30 mmol), and bpee (0.30 mmol) were combined with 15 mL of DMF (N,N-Dimethylformamide) in a sealed bomb reactor and heated at 150°C for 72 hours, after which the temperature was lowered to room temperature over the course of 10 hours. The resulting crystals were then immersed in methanol for 3 days and dichloromethane for 4 days, after which they were placed under vacuum at room temperature overnight to afford the activated sample. Powder X-ray diffraction analysis was used to confirm phase purity and structural stability throughout the activation process (Fig. S1). All reagents were purchased from Sigma Aldrich and used without further purification.

III. RESULTS & DISCUSSION

The photoluminescent RPM3-Zn is a known sensor for the explosive precursor compound DNT, which adsorbs in the RPM3-Zn pore as depicted in Fig. 2a. Slight distortions of the RPM3-Zn structure are observed when the guest molecule is introduced, such as subtle rotations of the bpdc linker carbon rings, minor increases in

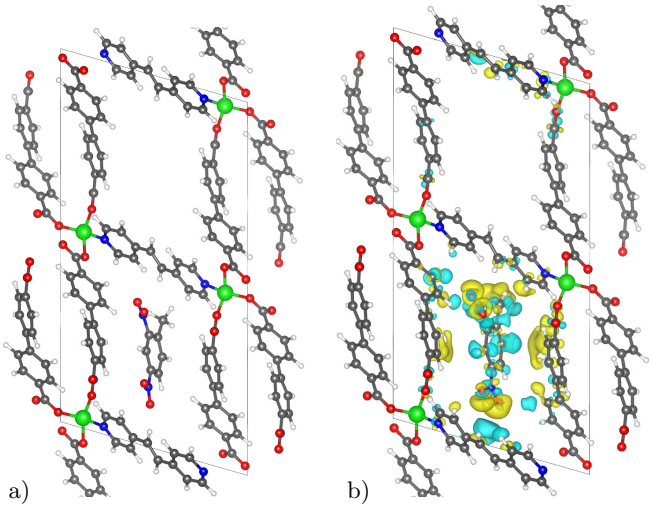

Figure 2. (a) DNT in the pore of the RPM3-Zn. (b) Induced charge rearrangement upon adsorption of the guest at an isosurface value of 5×10^{-4} $e/\text{Å}^3$. Yellow indicates a gain of charge and blue a loss of charge.

the size of the pore, and slight variations of the O–Zn–O bond angles. The average closest distance between the DNT molecule and bpee linker is 2.55 Å. Figure 2b shows the charge density rearrangement induced by the guest molecule. Some, albeit little, charge sharing between the guest molecule and MOF is visible (note the small isovalue), which is indicative of long-range van der Waals interactions between the guest molecule and the MOF structure. Inside the DNT molecule, the charge slightly rearranges, accumulating at the NO_2 branches and depleting in the phenyl ring.

The HOMO and LUMO orbitals are visualized in Fig. S2 using band decomposed charge densities. The RPM3-Zn HOMO is on the bpdc ligand while the LUMO is a set of two degenerate bpee ligand orbitals. Interestingly, upon adsorption of the DNT guest molecule, the LUMO (referred to as LUMO_{DNT}) switches to a set of two DNT orbitals, which are inserted into the RPM3-Zn band gap and the HOMO (referred to as HOMO_{DNT}) localizes on the opposite, unoccupied pore, spatially separating HOMO_{DNT} and LUMO_{DNT} significantly. The LUMO_{DNT} is mostly localized on the NO_2 groups which face the bpee ligands, i.e. the LUMO of the empty RPM3-Zn. The charge rearrangement in Fig. 2b and the closeness of the NO_2 groups to the bpee ligands suggests a noticeable interaction between DNT and the bpee ligand. To verify this interaction experimentally, IR spectra were taken for solid DNT, RPM3-Zn, and DNT+RPM3-Zn and the results are depicted in Fig. 3. Characteristic DNT peaks[48] clearly appear in the DNT+RPM3-Zn spectrum and slightly decay after evacuation (Fig. S3), confirming that the DNT is adsorbed into RPM3-Zn. The difference spectrum, which is the DNT+RPM3-Zn minus the RPM3-Zn spectrum, helps identify the exact wavenumbers of the DNT modes inside the MOF, as the interfering linker modes are subtracted out. The interaction of DNT with the bpee ligand can be seen through its fingerprint of clear red shifts in the $\nu_{\text{as}}(NO_2)$ and $\nu_{\text{s}}(NO_2)$ modes of 17 and 5 cm^{-1}, respectively, and a blue shift in the ν(C–N) mode of -19 cm^{-1}. The mode assignments and amount of shifts were further verified with high accuracy via DFT calculations, see Table S1. Characteristic modes of the RPM3-Zn bpee ligand[4,46] and bpdc ligand[4,47] are also identified in Fig. 3. While slight perturbations are noted for several modes—likely due to the closeness of the adsorbed DNT—two significant valleys appear in the difference spectrum for the ν(C=C–H) and ν(C=C) bpee modes at 1212 cm^{-1} and 1639 cm^{-1}, respectively. Whether the latter is attributed to a shift in frequency position or a decrease in intensity cannot be conclusively determined. These results constitute spectroscopic evidence for the interaction of DNT with the bpee ligand mentioned in our prior analysis. Aside from the perturbation observed for the ν(C=C–H) bpdc mode around 1170 cm^{-1} in the difference spectrum, the bpdc linker seems mostly undisturbed by the presence of DNT, suggesting that their interaction is weak.

Measured and calculated photoluminescence spectra of RPM3-Zn and DNT+RPM3-Zn are depicted in Fig. 4 (with absorption spectra shown in Fig. S4). Using the maximum value of the curve, we calculate that DNT quenches the photoluminescence of RPM3-Zn by 73%, which is in excellent agreement with the experimental value of 81% and validates our computational methodology. This result also reaffirms that the radiative relaxation of an electron between the bpee ligand LUMO and the bpdc ligand HOMO after a photoexcitaiton is what drives this luminescence. It is clear that the DNT orbitals disrupt the energetic structure of the RPM3-Zn system—however, it is not immediately clear what process drives the photoluminescent quenching. Several conjectures have been proposed in the literature: **1**) the DNT molecule increases the amplitude of the vibronic motion of the RPM3-Zn ions, which may decrease photoluminescence, **2**) the DNT introduces a trap state when adsorbed in the RPM3-Zn system, or **3**) the DNT molecule acts as an acceptor of charge (an electron) or energy during the non-radiative relaxation process. In the following, we will analyze and prove/disprove each possibility individually.

In order to study possibility **1**, the ionic vibrations were analyzed throughout the 1000 time steps of our MD trajectory and the atomic displacement parameters were calculated. To simulate different levels of vibrations, we modeled the RPM3-Zn system at $T = 50$ K, 300 K, and 550 K. The results are depicted in Fig. S6 in the form of thermal ellipsoid images at the 99% probability level. As expected, the increased temperature results in significantly larger vibrations of the RPM3-Zn ions, but when we calculate the corresponding photoluminescence intensity, we see no quenching at all with an increase in vibronic motion, and the level remains constant to within 3% when comparing the 300 and 550 K simulations. This

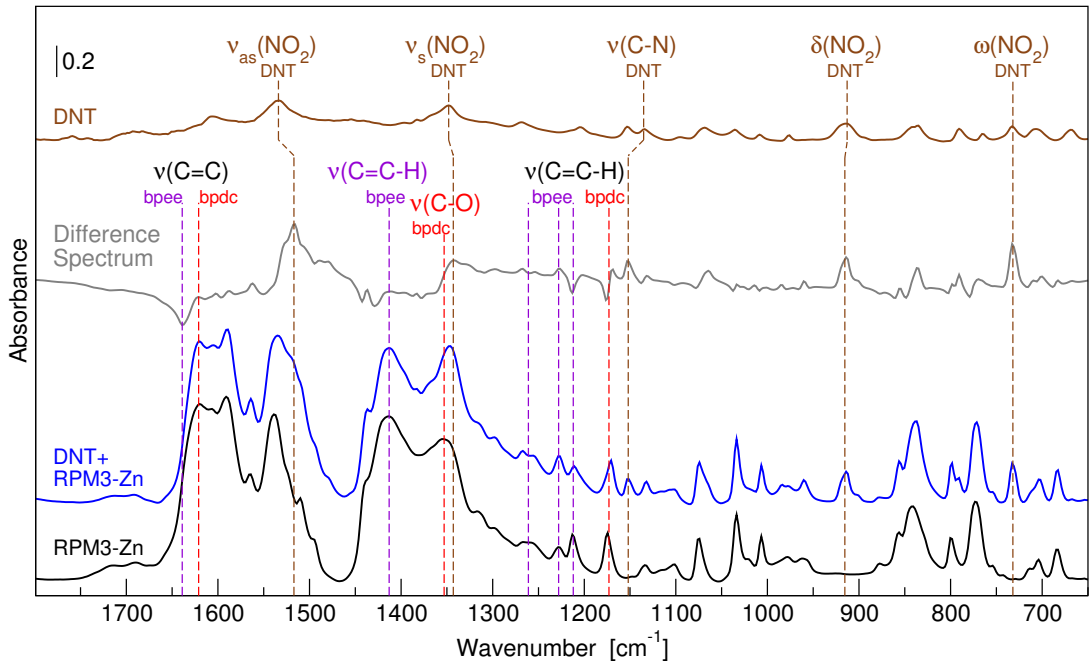

Figure 3. IR spectra of RPM3-Zn (black), DNT+RPM3-Zn (blue), and their difference spectrum (grey) along with solid DNT (brown). Important peaks are labeled for the RPM3-Zn bpee ligand[4,46] (purple), bpdc ligand[4,47] (red), and the DNT[48] molecule (brown). Selected wavenumbers are listed in Tables S1 and S2 along with the experimental and calculated shifts of the DNT modes.

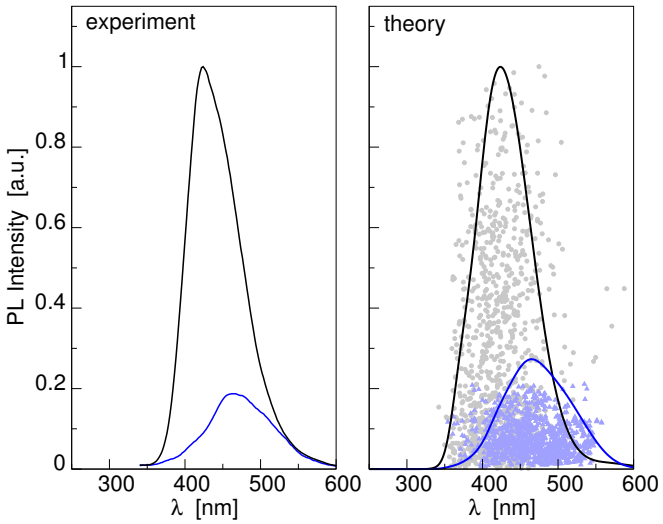

Figure 4. Photoluminescence spectrum for RPM3-Zn (black) and DNT+RPM3-Zn (blue) for a photoexcitaion of 320 nm (3.87 eV). The maximum of the RPM3-Zn line is normalized to 1 in both cases. The faded symbols in the background show the calculated f_{ij} values for the entire MD trajectory, which are also plotted separately in Fig. S5.

result shows that increasing the vibration of the RPM3-Zn *by itself does not* cause a quenching of the photoluminescence. However, vibrations do play a crucial role. When comparing the RPM3-Zn and DNT+RPM3-Zn systems in Fig. S7, we see that the bpee linker vibrations do increase noticeably in the presence of the DNT guest molecule, while the rest of the MOF system is largely unaffected. As discussed above, the DNT molecule has a noticeable interaction with the bpee linker, which results in the increased vibronic coupling. Monitoring the distance between DNT and the bpee linker over the course of our MD simulation, we find that—while the average value is 2.55 Å—it can go down to as little as 2.05 Å, facilitating charge transfer that eventually leads to the quenching discussed in detail below.

In order to analyze the remaining two possibilities, the non-adiabatic electronic coupling methodology is used, allowing for the study of an artificial photoexcitation and subsequent electron/hole relaxation and pathways through energy and real space. We address possibility **2** by looking for electronic trap states that the DNT might have introduced, focusing on high-energy excitations across the largest amount of states. All transitions consistent with our calculated orbital energies in the experimentally studied range of 240 – 350 nm are analyzed, corresponding to excitations from 3.54 eV to 4.96 eV. Amongst the possible transitions for a particular energy, we only focus on the one with the highest oscillator strength. At the very high energetic end (260 nm), in the RPM3-Zn system an electron is excited from the HOMO^{-5} to the deep conduction band state LUMO^{+5}, from where it undergoes ultrafast relaxation (on the 10^{-2} to 10^{-1} ps timescale) to the LUMO^{+2} state (Fig. S8). At the same time, the hole relaxes from HOMO^{-5} to the HOMO. This configuration is stable

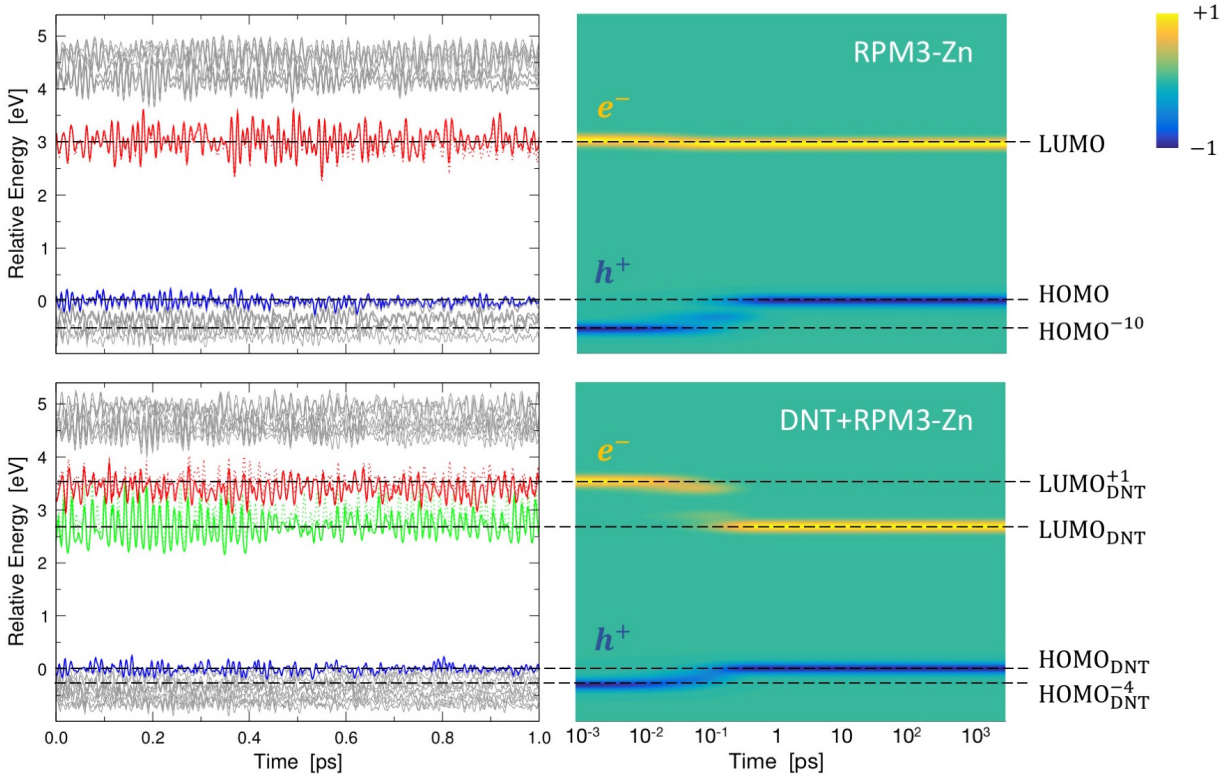

Figure 5. (left) Orbital energy fluctuation along the MD trajectory. The DNT molecule contributes orbitals (green line) in the gap of the original RPM3-Zn system (between the blue and red line), forming the new $LUMO_{DNT}$ of the combined DNT+RPM3-Zn system. The LUMO, $LUMO_{DNT}$, and $LUMO^{+1}_{DNT}$ orbitals are doubly degenerate (the ionic vibrations of the MD simulations slightly lift that degeneracy), indicated by corresponding solid and dotted lines. Plots are aligned such that the timed-average of HOMO and $HOMO_{DNT}$ are at zero. (right) Electron and hole relaxation after a 320 nm (3.87 eV) photoexcitation. Yellow indicates a gain of an electron, blue indicates a loss of an electron (i.e. hole), and green indicates no change in charge.

for up to 10^2 ps. Thereafter, the electron relaxes from $LUMO^{+2}$ to LUMO, from where it eventually photoluminesces on the ns timescale. Upon introduction of the DNT molecule, the pathway is essentially the same, albeit the excitation starts from slightly different orbitals ($HOMO^{-4}_{DNT}$ to $LUMO^{+4}_{DNT}$). Interestingly, when the electron relaxes, it skips the $LUMO^{+1}_{DNT}$ state—which corresponds to the LUMO state in the pristine RPM3-Zn system. Overall, no trap states are found and electron relaxation happens in the DNT+RPM3-Zn system even faster, i.e. on the 10 ps timescale.

For possibility **3**, i.e. the guest molecule accepts the excited electron in its $LUMO_{DNT}$ orbital from where it later photoluminesces, a few criteria must be met: (i) The guest molecule has to be in spatial proximity to the electron donating ligand, resulting in sufficient orbital overlap and (ii) the non-radiative electron transfer must occur on the fs to ps timescale in order to cutoff the radiative bpee to bpdc electron/hole recombination on the ns timescale, i.e. the driving force of RPM3-Zn photoluminescence. For the first criterium, as shown above, the ionic vibrations of DNT and the bpee ligand cause nonadiabatic coupling (Fig. S7) that facilitates the charge transfer in that the DNT/bpee ligand distance can become as low as 2.05 Å, well within the spatial range of non-radiative charge transfer processes. The second criterium requires a deeper analysis. Experimentally, an excitation of 320 nm (3.87 eV) is used for the spectrum depicted in Fig. 4, but no difference in emission was noted for excitations between 240 and 350 nm due to a flat absorption peak in that range, suggesting that accepting orbitals for excitations within that range have little variation in their relaxation pathway.[34] As can be seen in Fig. 5, the closest calculated photoexcitation that correspond to 320 nm is $HOMO^{-10}$ to LUMO for RPM3-Zn and $HOMO^{-4}_{DNT}$ to $LUMO^{+1}_{DNT}$ for DNT+RPM3-Zn.

In both the RPM3-Zn and DNT+RPM3-Zn systems relaxation occurs on the 10^{-2} to 10^{-1} ps timescale. For comparison, gold clusters introduced in MOF pores (Au^{III}@MOF complexes) have significantly longer experimentally measured nonradiative relaxation rates around 50 μs.[49] The nonradiative relaxation seen in RPM3-Zn and DNT+RPM3-Zn is similar to that of computed rates of TiO_2 thin films (~1 ps)[50] and nanowires (~0.8 ps),[51,52] and comparable to the 1–25 ps range of the rates in a PL active lead halide quantum dot (PbSe

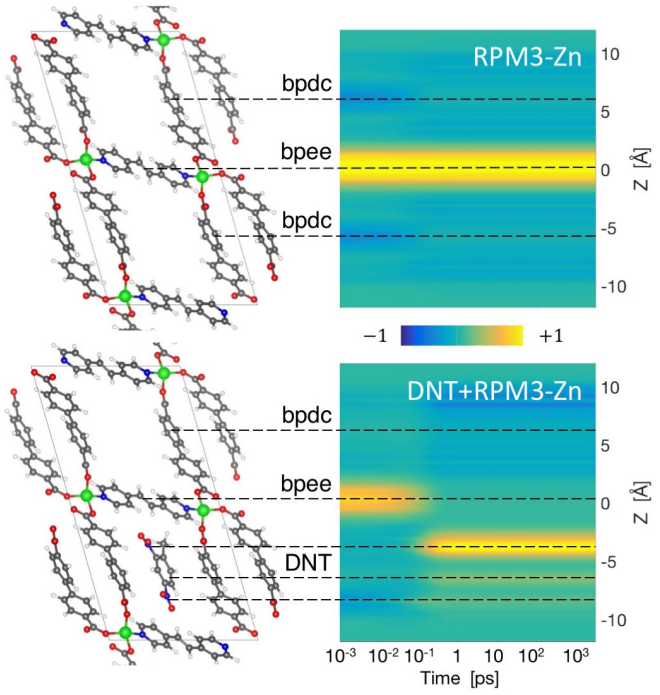

Figure 6. Real space electron and hole relaxation after a 320 nm (3.87 eV) photoexcitation. Yellow indicates a gain of an electron, blue indicates a loss of an electron (i.e. hole), and green indicates no change in charge. The plots are obtained by integrating the charge density in the xy-plane and showing the result for all z values in the unit cell as a function of time.

QD).[53] For the holes, the valence bands of each system are made up of densely packed bpdc orbitals, so the energetic and spatial relaxation pathways are uninhibited. Electron relaxation in the RPM3-Zn does not occur because the excitation is already to the LUMO. However, in the DNT+RPM3-Zn system, the electron gets excited into the $\mathrm{LUMO}^{+1}_{\mathrm{DNT}}$ state and then relaxes to the $\mathrm{LUMO}_{\mathrm{DNT}}$ state on the 10^{-1} ps timescale. Essentially, this is an electron transfer from the bpee ligand to the DNT molecule. Photoluminescence then happens from $\mathrm{LUMO}_{\mathrm{DNT}}$ to $\mathrm{HOMO}_{\mathrm{DNT}}$ on the ns timescale; however, it is quenched because the oscillator strengths for this transition are significantly smaller (see Fig. 4). Also, note that the gap in the DNT+RPM3-Zn system is smaller compared to the RPM3-Zn system, resulting in a lower energy transition and red shift of the spectrum in Fig. 4. The quick timescale of the electron relaxation in DFT+RPM3-Zn thus allows for quenched photoluminescence out of $\mathrm{LUMO}_{\mathrm{DNT}}$, cutting off the process before photoluminescence occurs out of $\mathrm{LUMO}^{+1}_{\mathrm{DNT}}$. The spatial charge rearrangement due to electron dynamics can also be seen in real space in Fig. 6. In the RPM3-Zn system the excitation of the electron is into the LUMO orbital, which is localized on the bpee ligand, and it remains there until it photoluminesces. The hole is at first localized on the bpdc ligand and on the order of 10^{-2} to 10^{-1} ps delocalizes somewhat, but nonetheless remains on that ligand. In the DNT+RPM3-Zn system the process is very similar, however, after 10^{-1} ps the electron relaxes to the DNT molecules (mostly to the NO_2 group) and remains there until it photoluminesces.

In summary, the mechanism of photoluminescence quenching upon DNT adsorption in RPM3-Zn is the following: The DNT molecule contributes an orbital into the gap of the original RPM3-Zn system. The excitation is in both cases to the bpee ligand, but in the DNT+RPM3-Zn system the electron relaxes to the DNT molecule on the 10^{-1} ps timescale. This relaxation is possible due to the relatively close proximity of the DNT and bpee ligand and is further enhanced through the normal modes of both; the periodic nuclear motion modifies the spatial overlap of the orbitals. The actual quenching then follows because of the reduced oscillator strength between the $\mathrm{LUMO}_{\mathrm{DNT}}$ (located on the DNT molecule) and $\mathrm{HOMO}_{\mathrm{DNT}}$ (located on the bpdc ligand), which is the result of the larger spatial separation of these orbitals.

IV. CONCLUSIONS

We present a methodology suitable to provide an in-depth analysis of what causes photoluminescence quenching upon guest-molecule adsorption in MOFs. We show that adsorption of DNT in RPM3-Zn causes a quenching of photoluminescence due to electron transfer from the photoexcited MOF to the guest molecule during the relaxation process. The guest is directly involved in the mechanism of quenching and, while no direct bond occurs with the MOF, the proximity between the guest and the host allows for non-radiative relaxation to the guest $\mathrm{LUMO}_{\mathrm{DNT}}$ due to spatial orbital overlap, cutting off the radiative relaxation pathway and electron/hole recombination between the organic linkers of the MOF which drives the photoluminescence without the guest present. While our methodology is tested on a single system, we believe that it is widely applicable to study photoluminescence phenomena in other MOFs and even other classes of materials, with significant implications for the design of more sensitive and specific sensors.

ACKNOWLEDGMENTS

This work was entirely supported by the Department of Energy Grant No. DE-FG02-08ER46491.

* These authors contributed equally

† E-mail: thonhauser@wfu.edu

[1] J. Liu, P. K. Thallapally, B. P. McGrail, D. R. Brown, and J. Liu, Chem. Soc. Rev. **41**, 2308 (2012).
[2] L. J. Murray, M. Dinca, and J. R. Long, Chem. Soc. Rev. **38**, 1294 (2009).
[3] J.-R. Li, Y. Ma, M. C. McCarthy, J. Sculley, J. Yu, H.-K. Jeong, P. B. Balbuena, and H.-C. Zhou, Coord. Chem. Rev. **255**, 1791 (2011).
[4] N. Nijem, H. Wu, P. Canepa, A. Marti, K. J. Balkus, T. Thonhauser, J. Li, and Y. J. Chabal, J. Am. Chem. Soc. **134**, 15201 (2012).
[5] K. Lee, J. D. Howe, L.-C. Lin, B. Smit, and J. B. Neaton, Chem. Mater. **27**, 668 (2015).
[6] D. Zhao, D. Yuan, and H.-C. Zhou, Energy Environ. Sci. **1**, 222 (2008).
[7] N. L. Rosi, J. Eckert, M. Eddaoudi, D. T. Vodak, J. Kim, M. O'Keeffe, and O. M. Yaghi, Science **300**, 1127 (2003).
[8] H. Wu, Q. Gong, D. H. Olson, and J. Li, Chem. Rev. **112**, 836 (2012).
[9] Y. He, W. Zhou, G. Qian, and B. Chen, Chem. Soc. Rev. **43**, 5657 (2014).
[10] C.-D. Wu and W. Lin, Angew. Chem. Int. Ed. **46**, 1075 (2007).
[11] J. Lee, O. K. Farha, J. Roberts, K. A. Scheidt, S. T. Nguyen, and J. T. Hupp, Chem. Soc. Rev. **38**, 1450 (2009).
[12] R.-Q. Zou, H. Sakurai, and Q. Xu, Angew. Chemie Int. Ed. **45**, 2542 (2006).
[13] I. Luz, F. X. Llabrés i Xamena, and A. Corma, J. Catal. **276**, 134 (2010).
[14] P. Horcajada, T. Chalati, C. Serre, B. Gillet, C. Sebrie, T. Baati, J. F. Eubank, D. Heurtaux, P. Clayette, C. Kreuz, J.-S. Chang, Y. K. Hwang, V. Marsaud, P.-N. Bories, L. Cynober, S. Gil, G. Férey, P. Couvreur, and R. Gref, Nat. Mater. **9**, 172 (2010).
[15] M. D. Allendorf, C. A. Bauer, R. K. Bhakta, and R. Houk, Chem. Soc. Rev. **38**, 1330 (2009).
[16] K. A. White, D. A. Chengelis, K. A. Gogick, J. Stehman, N. L. Rosi, and S. Petoud, J. Am. Chem. Soc. **131**, 18069 (2009).
[17] A. Stroppa, P. Jain, P. Barone, M. Marsman, J. M. Perez-Mato, A. K. K. Cheetham, H. W. Kroto, and S. Picozzi, Angew. Chem. Int. Ed. **50**, 5847 (2011).
[18] A. Stroppa, P. Barone, P. Jain, J. M. Perez-Mato, and S. Picozzi, Adv. Mater. **25**, 2284 (2013).
[19] D. Di Sante, A. Stroppa, P. Jain, and S. Picozzi, J. Am. Chem. Soc. **135**, 18126 (2013).
[20] S. E. Miller, M. H. Teplensky, P. Z. Moghadam, and D. Fairen-Jimenez, Interface Focus **6**, 20160027 (2016).
[21] P. Canepa, K. Tan, Y. Du, H. Lu, Y. J. Chabal, and T. Thonhauser, J. Mater. Chem. A **3**, 986 (2015).
[22] L. E. Kreno, K. Leong, O. K. Farha, M. Allendorf, R. P. Van Duyne, and J. T. Hupp, Chem. Rev. **112**, 1105 (2012).
[23] C. Serre, C. Mellot-Draznieks, S. Surblé, N. Audebrand, Y. Filinchuck, and G. Férey, Science **315**, 1828 (2007).
[24] M. D. Allendorf, R. J. T. Houk, L. Andruskiewicz, A. A. Talin, J. Pikarsky, A. Choundhury, K. A. Gall, and P. J. Hensketh, J. Am. Chem. Soc. **130**, 14404 (2008).
[25] J.-C. Tan and A. K. Cheetham, Chem. Soc. Rev. **40**, 1059 (2011).
[26] Z. Hu, B. J. Deibert, and J. Li, Chem. Soc. Rev. **43**, 5815 (2014).
[27] K. Müller-Buschbaum, F. Beuerle, and C. Feldmann, Micropor. Mesopor. Mat. **216**, 171 (2015).
[28] L. E. Kreno, K. Leong, O. K. Farha, M. Allendorf, R. P. Van Duyne, and J. T. Hupp, Chem. Rev. **112**, 1105 (2011).
[29] R.-B. Lin, S.-Y. Liu, J.-W. Ye, X.-Y. Li, and J.-P. Zhang, Adv. Sci. **3**, 1500434 (2016).
[30] W. P. Lustig, S. Mukherjee, N. D. Rudd, A. V. Desai, J. Li, and S. K. Ghosh, Chem. Soc. Rev. **46**, 3242 (2017).
[31] S. Pramanik, C. Zheng, X. Zhang, T. J. Emge, and J. Li, J. Am. Chem. Soc. **133**, 4153 (2011).
[32] Z. Hu, K. Tan, W. P. Lustig, H. Wang, Y. Zhao, C. Zheng, D. Banerjee, T. J. Emge, Y. J. Chabal, and J. Li, Chem. Sci. **5**, 4873 (2014).
[33] M. Kasha, Discussions of the Faraday Society **9**, 14 (1950).
[34] A. Lan, K. Li, H. Wu, D. H. Olson, T. J. Emge, W. Ki, M. Hong, and J. Li, Angew. Chem. Int. Ed. **48**, 2334 (2009).
[35] G. Kresse and J. Furthmüller, Phys. Rev. B **54**, 11169 (1996).
[36] G. Kresse and D. Joubert, Phys. Rev. B **59**, 1758 (1999).
[37] K. Berland, V. R. Cooper, K. Lee, E. Schröder, T. Thonhauser, P. Hyldgaard, and B. I. Lundqvist, Reports Prog. Phys. **78**, 066501 (2015).
[38] D. C. Langreth, B. I. Lundqvist, S. D. Chakarova-Käck, V. R. Cooper, M. Dion, P. Hyldgaard, A. Kelkkanen, J. Kleis, L. Kong, S. Li, P. G. Moses, E. D. Murray, A. Puzder, H. Rydberg, E. Schröder, and T. Thonhauser, J. Phys. Condens. Matter **21**, 084203 (2009).
[39] T. Thonhauser, V. R. Cooper, S. Li, A. Puzder, P. Hyldgaard, and D. C. Langreth, Phys. Rev. B **76**, 125112 (2007).
[40] T. Thonhauser, S. Zuluaga, C. A. Arter, K. Berland, E. Schröder, and P. Hyldgaard, Phys. Rev. Lett. **115**, 136402 (2015).
[41] D. J. Vogel and D. S. Kilin, J. Phys. Chem. C **119**, 27954 (2015).
[42] J. Heyd and G. E. Scuseria, J. Chem. Phys. **124**, 219906 (2006).
[43] A. J. Garza and G. E. Scuseria, J. Phys. Chem. Lett. **7**, 4165 (2016).
[44] J. Chen, A. Schmitz, T. Inerbaev, Q. Meng, S. Kilina, S. Tretiak, and D. S. Kilin, J. Phys. Chem. Lett. **4**, 2906 (2013).
[45] K. L. Svane and A. Walsh, J. Phys. Chem. C **121**, 421 (2017).
[46] Z. Özhamam, M. Yurdakul, and Ş. Yurdakul, J. Mol. Struct. Theochem **761**, 113 (2006).
[47] S. Mohr, T. Schmitt, T. Döpper, F. Xiang, M. Schwarz, A. Görling, M. A. Schneider, and J. Libuda, Langmuir **33**, 4178 (2017).
[48] G. Andreev, B. Jordanov, I. Juchnovski, and B. Schrader, J. Mol. Struct. **115**, 375 (1984).
[49] C.-Y. Sun, W.-P. To, X.-L. Wang, K.-T. Chan, Z.-M. Su, and C.-M. Che, Chem. Sci. **6**, 7105 (2015).
[50] S. Jensen and D. S. Kilin, J. Phys. Condens. Matter **27**, 134207 (2015).
[51] S. Huang and D. S. Kilin, Mol. Phys. **112**, 539 (2014).
[52] S. J. Jensen, T. M. Inerbaev, A. U. Abuova, and D. S. Kilin, J. Phys. Chem. C **121**, 16110 (2017).
[53] D. J. Vogel, A. Kryjevski, T. Inerbaev, and D. S. Kilin, J. Phys. Chem. Lett. **8**, 3032 (2017).

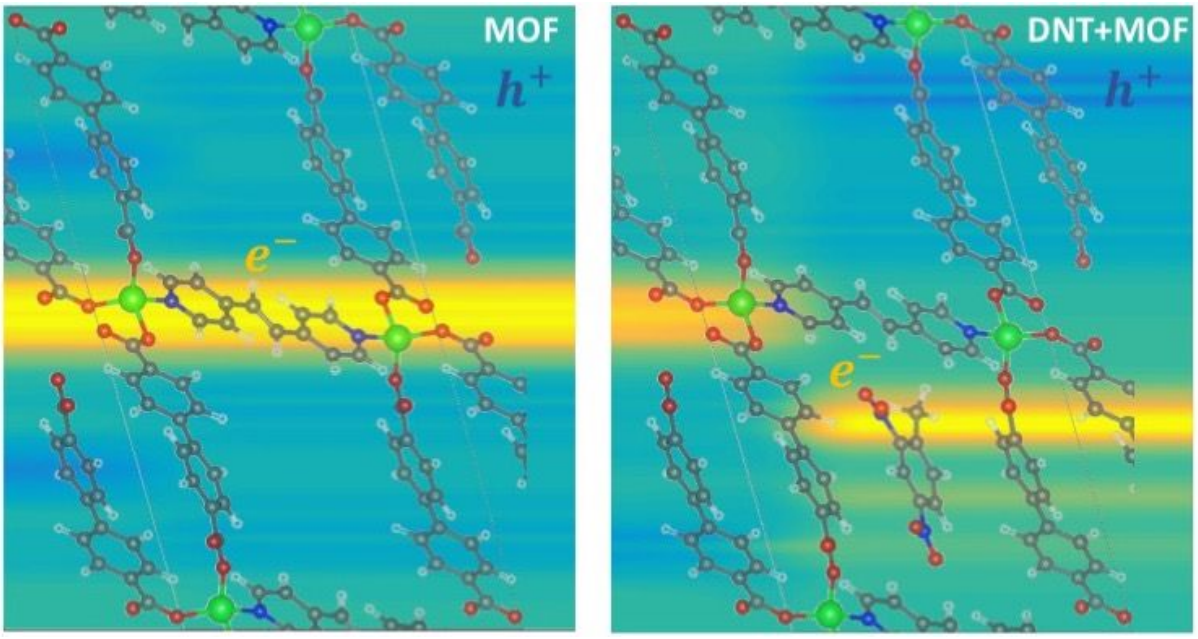

The electron transfer process from the MOF to the guest molecule (DNT), which quenches the photoluminescence of RPM3-Zn.